Nanostructures

DOI: 10.1002/ange.201403655

Copper-Based Ternary and Quaternary Semiconductor Nanoplates: Templated Synthesis, Characterization, and Photoelectrochemical Properties**

*Xue-Jun Wu, Xiao Huang, Xiaoying Qi, Hai Li, Bing Li, and Hua Zhang**

Abstract: *Two-dimensional (2D) copper-based ternary and quaternary semiconductors are promising building blocks for the construction of efficient solution-processed photovoltaic devices at low cost. However, the facile synthesis of such 2D nanoplates with well-defined shape and uniform size remains a challenge. Reported herein is a universal template-mediated method for preparing copper-based ternary and quaternary chalcogenide nanoplates, that is, $CuInS_2$, $CuIn_xGa_{1-x}S_2$, and Cu_2ZnSnS_4, by using a pre-synthesized CuS nanoplate as the starting template. The various synthesized nanoplates are monophasic with uniform thickness and lateral size. As a proof of concept, the Cu_2ZnSnS_4 nanoplates were immobilized on a Mo/glass substrate and used as semiconductor photoelectrode, thus showing stable photoelectrochemical response. The method is general and provides future opportunities for fabrication of cost-effective photovoltaic devices based on 2D semiconductors.*

Because of the increasing demand for clean energy, there has been growing interest in fabrication of photovoltaic devices which can harvest and directly convert solar energy into electricity.[1] Compared to other high-cost methods based on vacuum techniques for fabrication of photovoltaic devices, the solution-processing approach based on nanocrystal suspensions is particularly appealing because of its simplicity and lower cost.[2,3] One of the key issues in fabrication of solution-processible photovoltaic devices is the synthesis of inorganic nanocrystals with an appropriate band-gap for solar light absorption and conversion. In an effort to explore new materials suitable for photovoltaics, the field of design and synthesis of semiconducting nanocrystals, a field previously dominated by binary semiconductors, has been expanded to include more complex ternary and quaternary structures. Among them, copper-based ternary I-III-VI_2 semiconductors [e.g., $CuInS_2$ (CIS) and $CuIn_xGa_{1-x}S_2$ (CIGS)] and quaternary semiconductors [e.g., Cu_2ZnSnS_4 (CZTS)] are the most promising candidates because of their optimal band-gaps, large absorption coefficients, and high photostability.[4–6]

Until now, various synthetic routes, including the single-source decomposition, as well as hydrothermal and solvothermal reactions, have been developed for the synthesis of CIS[7–10] and CZTS[11–13] nanocrystals. However, compared to the common binary chalcogenides,[14] it is still difficult to control the stoichiometry and crystal phase of the ternary and quaternary nanocrystals because of the different reactivity of metal precursors and the complex interactions between the capping molecules and nanocrystals, which may result in the formation of biphasic nanomaterials or heterostructures as the intermediate products.[15–30] As one of the successful examples for preparing CIS nanostructures, the group of Cui reported the epitaxial growth of CIS nanorods on pre-nucleated Cu_2S nanodisks, followed by the progressive transformation of the biphasic Cu_2S-CIS into monophasic CIS nanorods.[24] Recently, the group of Xie reported that preformed CuSe can be used as a self-sacrificial template for preparation of ultrathin $CuInSe_2$ nanoplates, but the nanoplates showed small sizes with a broad size distribution.[30] The aforementioned investigations shed light on the transformation mechanism and complex phase behavior during the synthesis of ternary and quaternary semiconductor nanocrystals.

In addition to the crystal phase, the control over shape and size of ternary and quaternary semiconductors is also essential for tuning their optical properties.[31,32] Nanospheres and nanorods are the most common shapes observed in ternary and quaternary semiconductors which are synthesized in solutions. However, two-dimensional (2D) nanoplates of ternary and quaternary semiconductors have been rarely reported until now.[30,33–35] For example, the groups of Sargent and Li reported the synthesis of $CuInSe_2$ nanoplates through the specific choice of ligand and reaction temperature.[34,35] However, most of the obtained nanoplates showed either a wide size distribution or irregular shapes. Therefore, the facile synthesis of phase-pure ternary and quaternary nanoplates with well-defined shapes and narrow size distribution remains a big challenge.

[*] Dr. X.-J. Wu, Dr. X. Huang, Dr. H. Li, Prof. Dr. H. Zhang
School of Materials Science and Engineering
Nanyang Technological University
50 Nanyang Avenue, Singapore 639798 (Singapore)
E-mail: HZhang@ntu.edu.sg
Homepage: http://www.ntu.edu.sg/home/hzhang/
Dr. X. Y. Qi
Singapore Institute of Manufacturing Technology (SIMTech)
Singapore 638075 (Singapore)
Dr. B. Li
Institute of Materials Research and Engineering
Agency for Science, Technology and Research
Singapore 117602 (Singapore)

[**] This work was supported by MOE under AcRF Tier 2 (ARC 26/13, No. MOE2013-T2-1-034), AcRF Tier 1 (RG 61/12, RGT18/13, and RG5/13), and Start-Up Grant (M4080865.070.706022) in Singapore. This Research is also conducted by NTU-HUJ-BGU Nanomaterials for Energy and Water Management Programme under the Campus for Research Excellence and Technological Enterprise (CREATE), which is supported by the National Research Foundation, Prime Minister's Office, Singapore.

Supporting information for this article is available on the WWW under http://dx.doi.org/10.1002/anie.201403655.

Following our recent work on the phase transformation of copper selenides through a solution-phase process,[36] we herein present a facile and general template-based method for the synthesis of monodispersed ternary and quaternary semiconducting nanoplates. In our experiment, the ultrathin covellite-phase CuS nanoplates were chosen as the templates, and the corresponding ternary (e.g., CIS) and quaternary nanoplates (e.g., CIGS and CZTS) were successfully produced in a high-temperature solution reaction with appropriate metal precursors. The X-ray diffraction (XRD) and Raman spectra confirmed that the final products are monophasic without any impurity. Moreover, the template-mediated growth mechanism is discussed. The optical properties of the obtained various nanoplates and the photoelectrochemical properties of their thin films were also investigated.

As a typical example, the synthesis of the CIS nanoplate was chosen to illustrate the template-mediated transformation, in which the CuS nanoplate was used as the initial template synthesized based on our recently reported method.[36] Figures 1 a and b show the typical transmission electron microscopy (TEM) images of the obtained CuS nanoplates, which are hexagonal in shape with an average plane length of (150 ± 40) nm and thickness of about 4.8 nm, thus corresponding to three unit cells (the lattice constant of CuS along the *c* axis is 1.63 nm). After the CuS nanoplates reacted with the indium precursor (i.e., indium(III) 2,4-pentanedionate) at high temperature (260 °C) for 2 hours, CIS nanoplates were formed (see the detailed synthetic procedure in the Supporting Information). XRD analysis (see Figure S1 in the Supporting Information) confirmed that the CIS nanoplate has a pure tetragonal chalcopyrite structure (JCPDS, 65-1572), which is different from the commonly observed wurtzite phase.[21–28] Figure 1 c illustrates a scanning electron microscopy (SEM) image of the CIS nanoplates. It can be seen that all the nanocrystals maintained the 2D platelike shape and stacked face-to-face. The TEM image of a typical CIS nanoplate shows that it still possesses the hexagonal morphology (Figure 1 d), although its corners are not as sharp as that of the original CuS nanoplate. The observed interplane distances in the high-resolution TEM (HRTEM) images are about 0.32 and 0.19 nm (Figure 1 e,f) for the (112) and (220) planes, respectively, of chalcopyrite CIS, and also indicate that the CIS nanoplates are bound by {112} planes as the top and bottom surfaces. Furthermore, it was found that the thickness of the CIS nanoplates increased to about 12 nm from 4.8 nm of the original CuS nanoplates (Figure 1 e), while their average lateral size remained almost the same.

To study the mechanism of this template-mediated transformation, both crystal structures of the CuS template and CIS nanoplate are investigated. As shown in Figure 1 g, the initial hexagonal CuS nanoplate with the (001) basal plane transforms into the tetragonal CIS nanoplate with the (112) basal plane. It should be noted that the atomic arrangement of CuS (001) is similar with that of CIS (112) (middle panel of Figure 1 g). As viewed from the CuS (001) projection, the sulfur atoms are in regular hexagonal arrangement with Cu atoms located at the interstices. In contrast, the CIS (112) planes, which result from substituting half of Cu atoms in CuS with In atoms, deviate slightly from the perfect hexagonal symmetry because of the different atomic radii of Cu and In (Figure 1 g, middle panel). Despite the structural deviation, the in-plane lattice spacing of CIS is only slightly different from that of CuS, that is, the lattice spacing of $\{220\}_{CIS}$ and $\{204\}_{CIS}$ is larger than that of $\{110\}_{CuS}$ by only 3.0 and 3.3 %, respectively. The structural similarity between the CuS and CIS crystals ensured the successful transformation from CuS to CIS without the change of morphology. The most distinct difference between these two structures is that the CuS crystal consists of alternating CuS_3-Cu_3S-CuS_3 covalent layers and S–S van der Waals layers along the [001] direction,[37] while in the chalcopyrite CIS, every Cu and In atom is tetragonal-coordinated with sulfur atoms. Comparing the crystal structure of CuS along the *z* axis with that of CIS along [221] direction (bottom panel of Figure 1 g), it can be seen that during the transformation, as the In^{3+} ions insert into the S–S layers of CuS, formed by van der Waals interactions, and partially replace the initial Cu^{+} ions, the S planes also undergo a gliding motion to eventually transform to the tetragonal structure. In addition, the Cu^{+} ions which are replaced by In^{3+} ions will further react with the indium and sulfur precursors in solution to produce the newly formed CIS, which is re-deposited on the plane of the initial nanoplate. Note that half of the initial Cu^{+} ions are replaced by In^{3+} ions and dissolved into the solution to participate in the re-growth process, and the lattice spacing of planes parallel to the 2D basal plane expands by about 20 % after the CuS to CIS transformation (i.e. from $d_{(006)CuS} = 0.27$ nm to $d_{(112)CIS} = 0.32$ nm). As a result, the thickness

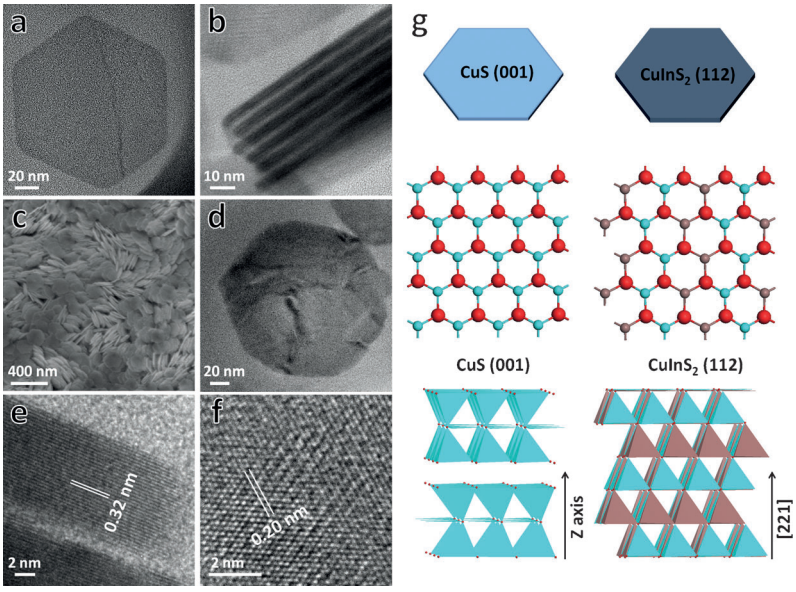

Figure 1. a,b) TEM images of CuS nanoplates. SEM (c) and TEM images (d–f) of $CuInS_2$ nanoplates prepared by the CuS-templated transformation. g) Structural models of (left) CuS and (right) $CuInS_2$.

of the CIS nanoplates is more than doubled (about 12 nm) compared to the original CuS template (about 4.8 nm).

Compared to our recently reported templated phase transformation of binary copper sulfide (e.g., from hexagonal CuS to djurleite $Cu_{1.97}S$ nanoplates),[36] the transformation from CuS to CIS here is more complicated. First, when In^{3+} ions are inserted into the CuS template, half of the initial Cu^+ ions need to be replaced to maintain the total charge balance, while in the CuS to $Cu_{1.97}S$ transition, the initial Cu^+ ions remain in the rigid sulfur framework when additional Cu^+ ions are inserted. Second, the thickness of CIS nanoplate is more than doubled compared to that of the initial CuS template because of the regrowth step and lattice expansion which accompany the replacement of Cu^+ with In^{3+}, whereas the transformation from CuS to $Cu_{1.97}S$ only leads to a slight thickness increase (ca. 20%). Lastly, the templated growth here requires higher reaction temperature because of the much lower ion mobility of In^{3+} relative to that of Cu^+ within the framework.

Impressively, our unique template-mediated synthetic method can be used to synthesize CIGS nanoplates with tunable compositions (i.e., x varies from 0 to 1 in $CuIn_xGa_{1-x}S_2$) through the reaction of pre-synthesized CuS nanoplates and indium/gallium precursors at different molar ratios (see the Supporting Information for detailed experimental procedures). The compositions of obtained products were confirmed by EDS characterization and summarized in Table S1. Figure 2a shows XRD patterns of the $CuIn_xGa_{1-x}S_2$ nanoplates with different compositions, that is, $x = 1$, 0.75, 0.50, 0.25, and 0 (from bottom to top pattern). It can be found that the peak positions and the relative peak intensities match well with the chalcopyrite-type CIGS. Because of the smaller size of the Ga^{3+} ion as compared to the In^{3+} ion, a gradual peak shift to higher angle can be observed with an increase in Ga content in $CuIn_xGa_{1-x}S_2$. For example, the strongest (112) peak shifts from about 27.90° for CIS to approximately 29.06° for CGS when the Ga content is increased from 0 to 100%. Large-area SEM images confirmed that all the CIGS products are 2D nanoplates (see Figure S2). In the synthesized product of CGS (Figure S2e), spherical nanoparticles arising from the additional nucleation in the bulk solution were also observed, and coexisted with 2D nanoplates. To identify the elemental distribution of the nanoplates, STEM-EDS analysis was performed. The dark-field image of a single $CuIn_{0.5}Ga_{0.5}S_2$ nanoplate shows uniform contrast (Figure 2b), and the corresponding EDS elemental mapping reveals the homogeneous distribution of Cu, In, Ga and S elements, thus indicating that no phase separation occurred during the templated growth of $CuIn_{0.5}Ga_{0.5}S_2$ nanoplates. The STEM-EDS analyses of CIGS nanoplates with other compositions also suggested the monophasic nature of the products (see Figure S3).

More importantly, we found that the optical properties of the CIGS nanoplate are dependent upon the Ga (or In) content. With an increase in the Ga content, the color of the CIGS nanoplate suspension in *n*-hexane gradually changes from dark-brown to orange (inset of Figure 2b, from left to right, $x = 1$, 0.75, 0.5, 0.25 and 0 in $CuIn_xGa_{1-x}S_2$). Indeed, the UV/Vis extinction spectra of the corresponding CIGS suspensions showed substantial a blue shift of the optical absorbance band edge with increasing Ga content. The calculated optical band gaps from the diffuse reflectance spectra also gradually shifted to higher energy when the composition of $CuIn_xGa_{1-x}S_2$ was tuned from CIS to CGS (see Figure S4).

Impressively, our template-mediated method can be used to synthesize the quaternary Cu_2ZnSnS_4 (CZTS) nanoplate by complete replacement of In^{3+} ions with Zn^{2+} and Sn^{4+} ions. Actually, the CZTS crystal exhibits two phases, that is, stannite and kesterite, which depend on the occupancy positions of the cations.[38,39] However, it is difficult to distinguish them, as both phases may coexist because of the similar lattice parameters and total energy. Figures 3a and b show TEM images of prepared CZTS nanoplates, which are about 12 nm in thickness and (150 ± 40) nm in plane size. These nanoplates also preserve the hexagonal shape, similar to the initial CuS nanoplates. The observed lattice spacings are about 0.31 and 0.19 nm (Figure 3c and d), thus corresponding to the (112) and (220), respectively, planes of tetragonal CZTS structure. The EDS analysis verified that the nanoplate is composed of Cu, Zn, Sn, and S elements (see Figure S5). STEM-EDS elemental mapping of a typical nanoplate further demonstrates that the four elements are evenly distributed in the nanoplate (Figure 3e). The XRD analysis (Figure 3f) suggests that the obtained product can be assigned to the tetragonal structure with the kesterite phase (JCPDS, 26-0575). However, these

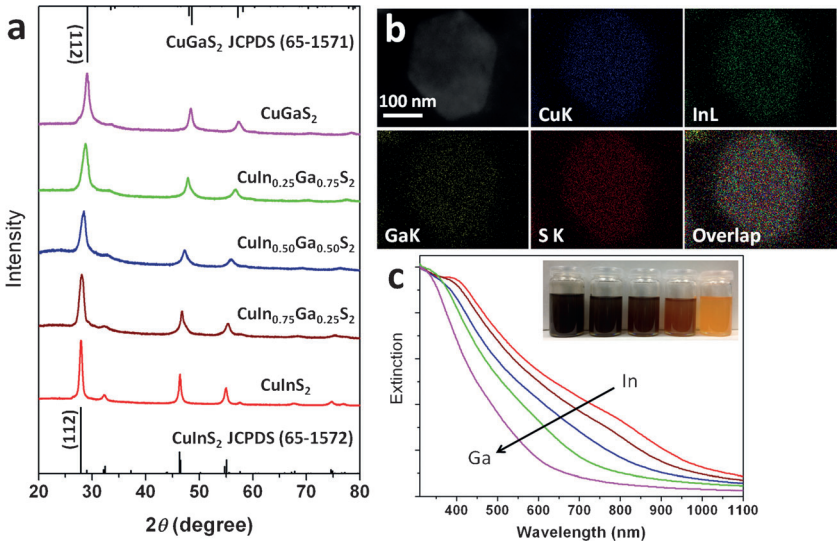

Figure 2. a) XRD patterns of $CuIn_xGa_{1-x}S_2$ nanoplates. b) STEM dark-field image of a single $CuIn_{0.50}Ga_{0.50}S_2$ nanoplate and the corresponding EDS mapping of the nanoplate. c) UV/Vis extinction spectra of the $CuIn_xGa_{1-x}S_2$ nanoplates. Inset: photograph of solutions of $CuIn_xGa_{1-x}S_2$ nanoplates with different compositions dispersed in *n*-hexane. From left to right, x in $CuIn_xGa_{1-x}S_2$ is equal to 1, 0.75, 0.50, 0.25, and 0, respectively.

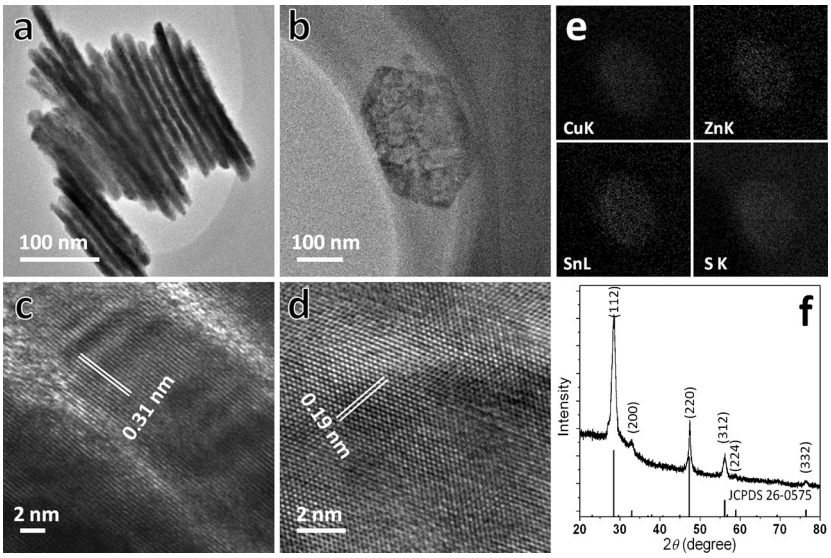

Figure 3. TEM (a,b) and HRTEM (c,d) images of synthesized CZTS nanoplates. e) STEM-EDS mapping of a single CZTS nanoplate shown in Figure 1 b. f) XRD pattern of CZTS nanoplates.

diffraction peaks can also be indexed to the combination of zinc blend ZnS and tetragonal Cu_2SnS_3. To confirm the phase purity of the CZTS nanoplate, Raman spectrum of the product was studied (see Figure S6). A relatively strong peak at about 336 cm^{-1} and a weak peak at approximately 284 cm^{-1} were observed, and are in agreement with those of bulk CZTS.[41] Meanwhile, the characteristic Raman peak of zinc blend ZnS at 356 cm^{-1} was absent, and excludes the presence of ZnS in the product. Therefore, the XRD peaks (Figure 3 f) cannot be assigned to the mixture of ZnS and Cu_2SnS_3, and we can confirm that the tetragonal CZTS is the only crystal phase present in the product.

Recently, the CZTS has been suggested as a promising building block for fabrication of solar cells because of its abundance and low cost.[40] To demonstrate the potential application of our 2D CZTS nanoplates in solar harvesting, the potoelectrochemical behavior of the 2D CZTS nanoplates immobilized on Mo/glass was characterized in the presence of 0.1 M $Eu(NO_3)_3$, which was used as the electron scavenger. The CZTS suspension shows strong photoabsorption in the entire visible range of light (see Figure S7), thus demonstrating their potential application as a light-absorbing layer. As shown in Figure 4, the cathodic photocurrent was detected at negative potentials (vs. Ag/AgCl), and the current magnitude increased as the electrode potential shifted to a more negative value. This observation indicates that the CZTS film behaved as p-type semiconducting photoelectrode. The stability of the photocurrent generated from the as-deposited CZTS thin film was evaluated at a constant potential of −0.5 V (vs. Ag/AgCl) at the light-on and light-off time of 10 seconds (inset of Figure 4). The CZTS film showed a constant photocurrent density of 0.07 mA cm^{-2} which remained stable over several minutes during the test despite being immersed in an aqueous electrolyte.

In summary, a facile and general method for the templated synthesis of copper-based ternary and quaternary nanoplates is reported. By using the synthesized CuS nanoplates as synthetic templates, the corresponding ternary and quaternary (e.g., $CuInS_2$, $CuIn_xGa_{1-x}S_2$, and Cu_2ZnSnS_4) nanoplates were successfully prepared through solution-based routes at high temperature. These nanoplates maintained the hexagonal shape of the initial CuS nanoplates, and showed lateral length of over one hundred nanometers and a thickness of about 12 nm. The successful realization of the template-mediated transformation between hexagonal-phase CuS and tetragonal-phase copper-based chalcogenides (i.e. CIGS or CZTS) mainly resulted from their structural similarity. As a proof of concept, the thin film prepared from CZTS nanoplates coated on a Mo/glass substrate was used as a photoelectrode, which exhibited similar photoelectrochemical activity to that of other p-type semiconductors in aqueous solution with $Eu(NO_3)_3$ as an electron scavenger. It is anticipated that the combination of these 2D p-type semiconductors with other n-type semiconductors through layer-by-layer deposition can produce novel inorganic multilayers, thus leading to highly efficient solar light conversion.

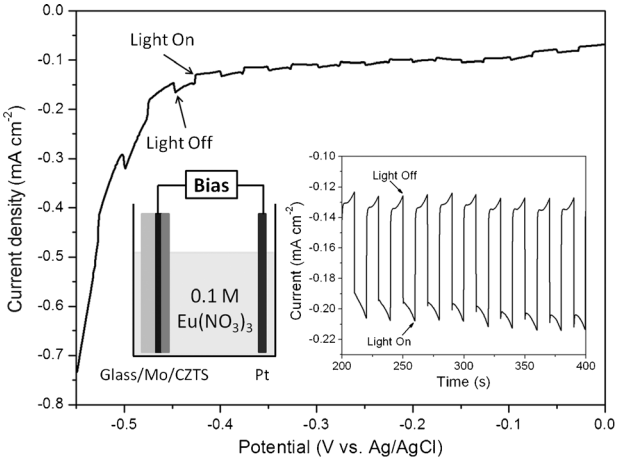

Figure 4. Plot of current density versus potential for the photocurrent response of Cu_2ZnSnS_4 nanoplate film immobilized on a Mo/glass substrate. Inset: The sketch map of the photoelectrochemical system and photostability measurement of Cu_2ZnSnS_4 film at a potential of −0.5 V (vs. Ag/AgCl).

Received: March 24, 2014
Published online: June 27, 2014

Keywords: copper · electron microscopy · nanomaterials · photovoltaic devices · template synthesis

[1] A. Shah, P. Torres, R. Tscharner, N. Wyrsch, H. Keppner, *Science* **1999**, *285*, 692 – 698.
[2] I. Gur, N. A. Fromer, M. L. Geier, A. P. Alivisatos, *Science* **2005**, *310*, 462 – 465.
[3] E. H. Sargent, *Nat. Photonics* **2009**, *3*, 325 – 331.
[4] M. I. Alonso, K. Wakita, J. Pascual, M. Garriga, N. Yamamoto, *Phys. Rev. B* **2001**, *63*, 075203.
[5] J.-F. Guillemoles, U. Rau, L. Kronik, H.-W. Schock, D. Cahen, *Adv. Mater.* **1999**, *11*, 957 – 961.
[6] H. Katagiri, K. Saitoh, T. Washio, H. Shinohara, T. Kurumadani, S. Miyajima, *Sol. Energy Mater. Sol. Cells* **2001**, *65*, 141 – 148.
[7] S. L. Castro, S. G. Bailey, R. P. Raffaelle, K. K. Banger, A. F. Hepp, *J. Phys. Chem. B* **2004**, *108*, 12429 – 12435.
[8] J. J. Nairn, P. J. Shapiro, B. Twamley, T. Pounds, R. von Wandruszka, T. R. Fletcher, M. Williams, C. Wang, M. G. Norton, *Nano Lett.* **2006**, *6*, 1218 – 1223.
[9] J. Xiao, Y. Xie, Y. Xiong, R. Tang, Y. Qian, *J. Mater. Chem.* **2001**, *11*, 1417 – 1420.
[10] J. Xiao, Y. Xie, R. Tang, Y. Qian, *J. Solid State Chem.* **2001**, *161*, 179 – 183.
[11] K. Ramasamy, M. A. Malik, P. O'Brien, *Chem. Commun.* **2012**, *48*, 5703 – 5714.
[12] X. Lu, Z. Zhuang, Q. Peng, Y. Li, *Chem. Commun.* **2011**, *47*, 3141 – 3143.
[13] A. Singh, H. Geaney, F. Laffir, K. M. Ryan, *J. Am. Chem. Soc.* **2012**, *134*, 2910 – 2913.
[14] J. Joo, H. B. Na, T. Yu, J. H. Yu, Y. W. Kim, F. Wu, J. Z. Zhang, T. Hyeon, *J. Am. Chem. Soc.* **2003**, *125*, 11100 – 11105.
[15] H. Zhong, S. S. Lo, T. Mirkovic, Y. Li, Y. Ding, Y. Li, G. D. Scholes, *ACS Nano* **2010**, *4*, 5253 – 5262.
[16] H. Zhong, Y. Zhou, M. Ye, Y. He, J. Ye, C. He, C. Yang, Y. Li, *Chem. Mater.* **2008**, *20*, 6434 – 6443.
[17] F. M. Courtel, R. W. Paynter, B. Marsan, M. Morin, *Chem. Mater.* **2009**, *21*, 3752 – 3762.
[18] R. Xie, M. Rutherford, X. Peng, *J. Am. Chem. Soc.* **2009**, *131*, 5691 – 5697.
[19] W.-C. Huang, C.-H. Tseng, S.-H. Chang, H.-Y. Tuan, C.-C. Chiang, L.-M. Lyu, M. H. Huang, *Langmuir* **2012**, *28*, 8496 – 8501.
[20] K. Nose, Y. Soma, T. Omata, S. Otsuka-Yao-Matsuo, *Chem. Mater.* **2009**, *21*, 2607 – 2613.
[21] D. Pan, L. An, Z. Sun, W. Hou, Y. Yang, Z. Yang, Y. Lu, *J. Am. Chem. Soc.* **2008**, *130*, 5620 – 5621.
[22] X. Lu, Z. Zhuang, Q. Peng, Y. Li, *CrystEngComm* **2011**, *13*, 4039 – 4045.
[23] M. Kruszynska, H. Borchert, J. Parisi, J. Kolny-Olesiak, *J. Am. Chem. Soc.* **2010**, *132*, 15976 – 15986.
[24] S. T. Connor, C.-M. Hsu, B. D. Weil, S. Aloni, Y. Cui, *J. Am. Chem. Soc.* **2009**, *131*, 4962 – 4966.
[25] M. E. Norako, M. A. Franzman, R. L. Brutchey, *Chem. Mater.* **2009**, *21*, 4299 – 4304.
[26] Y. Qi, Q. Liu, K. Tang, Z. Liang, Z. Ren, X. Liu, *J. Phys. Chem. C* **2009**, *113*, 3939 – 3944.
[27] Y.-H. A. Wang, X. Zhang, N. Bao, B. Lin, A. Gupta, *J. Am. Chem. Soc.* **2011**, *133*, 11072 – 11075.
[28] A. Singh, C. Coughlan, F. Laffir, K. M. Ryan, *ACS Nano* **2012**, *6*, 6977 – 6983.
[29] Q. Li, L. Zhai, C. Zou, X. Huang, L. Zhang, Y. Yang, X. a. Chen, S. Huang, *Nanoscale* **2013**, *5*, 1638 – 1648.
[30] W. Bi, M. Zhou, Z. Ma, H. Zhang, J. Yu, Y. Xie, *Chem. Commun.* **2012**, *48*, 9162 – 9164.
[31] X. Peng, L. Manna, W. Yang, J. Wickham, E. Scher, A. Kadavanich, A. P. Alivisatos, *Nature* **2000**, *404*, 59 – 61.
[32] J. Hu, L.-s. Li, W. Yang, L. Manna, L.-w. Wang, A. P. Alivisatos, *Science* **2001**, *292*, 2060 – 2063.
[33] H. Liu, Z. Jin, W. Wang, J. Li, *CrystEngComm* **2011**, *13*, 7198 – 7201.
[34] H. Zhong, Y. Li, M. Ye, Z. Zhu, Z. Yi, C. Yang, Y. Li, *Nanotechnology* **2007**, *18*, 025602.
[35] J. Tang, S. Hinds, S. O. Kelley, E. H. Sargent, *Chem. Mater.* **2008**, *20*, 6906 – 6910.
[36] X.-J. Wu, X. Huang, J. Liu, H. Li, J. Yang, B. Li, W. Huang, H. Zhang, *Angew. Chem.* **2014**, *126*, 5183 – 5187; *Angew. Chem. Int. Ed.* **2014**, *53*, 5083 – 5087.
[37] W. Du, X. Qian, X. Ma, Q. Gong, H. Cao, J. Yin, *Chem. Eur. J.* **2007**, *13*, 3241 – 3247.
[38] C. R. A. Catlow, Z. X. Guo, M. Miskufova, S. A. Shevlin, A. G. H. Smith, A. A. Sokol, A. Walsh, D. J. Wilson, S. M. Woodley, *Philos. Trans. R. Soc. London Ser. A* **2010**, *368*, 3379 – 3456.
[39] C. Persson, *J. Appl. Phys.* **2010**, *107*, 053710.
[40] M. Himmrich, H. Haeuseler, *Spectrochim. Acta Part A* **1991**, *47*, 933 – 942.
[41] Q. Guo, G. M. Ford, W.-C. Yang, B. C. Walker, E. A. Stach, H. W. Hillhouse, R. Agrawal, *J. Am. Chem. Soc.* **2010**, *132*, 17384 – 17386.